CHIN. PHYS. LETT. Vol. 31, No. 2 (2014) 026802

Surface Morphology of GaAs/$In_{0.3}Ga_{0.7}As$ in an Elastic Field of Static Point Defects *

WU Ping-Ping(吴平平), GAO Fang-Liang(高芳亮), ZHANG Shu-Guang(张曙光)**, LI Guo-Qiang(李国强)**
State Key Laboratory of Luminescent Materials and Devices, South China University of Technology, Guangzhou 510641

(Received 7 June 2013)

The surface morphology InGaAs layers with In composition of 0.3 on GaAs (001) substrates are simulated by the phase field method. We investigate the influence of the strain field induced by static point defects on surface morphology of the InGaAs thin film. Our simulation demonstrates that the rms roughness of the thin film surface is strongly dependent on the density and magnitude of the randomly distributed point defects. Point defects near the thin film surface can produce a relatively large change of the surface morphology. The influences of thin film thickness on the surface morphology with different defect distributions are illustrated in the simulations. Additionally, a combination of experiment and theory is used to examine the influence of the defect density and magnitude on the surface morphology and roughness.

PACS: 68.55.−a, 81.15.Aa, 68.55.jd DOI: 10.1088/0256-307X/31/2/026802

Multi-junction solar cells, built as a stack of solar cells of different bandgaps, can reach the highest conversion efficiency in all types of any known photovoltaic technologies. Its high efficiency drives a rapid growing market demand with many potential applications. At present, the multi-junction Ⅲ–Ⅴ solar cell efficiency is reported to be beyond 40%.[1−4] It is noted that the most common three-junction design for this type of high efficiency solar cell utilizes a InGaP/InGaAs/Ge structure. However, to further enhance the efficiency of photovoltaic cells, the 1-eV junction is the key to promote the next-generation solar cell design.[5,6] An optional choice for the 1-eV junction is $In_{0.3}Ga_{0.7}As$.[7] However, it has a large misfit strain of 2% on GaAs substrates.[8,9] This misfit strain will induce non-ideal growth due to the fact that the thin film layer is relaxed by the introduction of high defect density.[10,11] Controlling the thin film surface roughness and improving the crystal quality are critical to the solar cell performance.

The reason that prevents forming a perfect crystal is the crystallographic defects, which can be classified into surface, line, and point defects by dimensions of the bounded imperfect region on the atomic scale.[12] Many experimental results, including molecular-beam epitaxy (MBE)[13−15] and metal organic vapor phase epitaxy (MOVPE),[16] show that dislocations and point defects can be reduced by controlling the growth temperature. Although point defects have a strong influence on the quality of the thin film/quantum well structure,[17] it is quite difficult in experiment to identify the role played by the point defects in the progress of crystal growth. The engineering of point defects in the InGaAs thin film can improve the quality of thin films and enhance the desired properties of photovoltaic materials.

The objective of this work is to examine the role of a static elastic field generated by point defects on the surface morphology of GaAs/InGaAs heterostructures by employing the phase field method. To describe the surface morphology of $In_{0.3}Ga_{0.7}As$ thin film on the GaAs (001) substrate, we introduce three conserved order parameters η_1, η_2 and η_3 to represent the volume fractions of gas, thin film and substrate phases in the phase field model, respectively, and the total volume fraction of the system is fixed,

$$\eta_1 + \eta_2 + \eta_3 = 1. \tag{1}$$

The interface between order parameters η_i and η_j is denoted as γ_{ij}. In the present study, we assume that the substrate phase η_3 is static, thus the profile of η_3 is set to be the one dimensional equilibrium profile,

$$\eta_3 = \frac{1}{2}\Big[\tanh\frac{1}{2}(y_{\rm sub} - y) + 1\Big], \tag{2}$$

where $y_{\rm sub}$ is the value of the y-coordinate at the substrate surface. Therefore, according to Eq. (1), we can choose η_2 as an independent phase field. For a conserved system, the temporal evolution of the phase field η_2 of the $In_{0.3}Ga_{0.7}As$ thin film is determined by the nonlinear Cahn–Hilliard equations,[18]

$$\frac{\partial \eta_2}{\partial t} = \nabla\Big[M\nabla\Big(\frac{\delta F_{\rm tot}}{\delta \eta_2}\Big)\Big], \tag{3}$$

where M is the dynamic coefficient, t is time, and $F_{\rm tot}$ is the total free energy of the system, which includes the chemical energy, the interfacial energy and the elastic energy,

$$F_{\rm tot} = F_{\rm chem} + F_{\rm inter} + F_{\rm elas}. \tag{4}$$

The calculations of chemical energy, interfacial energy and elastic energy with defects were described in detail in Refs. [19–21].

In the simulations, the chemical energy parameters are chosen to be $\omega_{12} = \omega_{13} = \omega_{23} = 1.0$, the surface energies and interfacial energy are $\alpha_{12} = \alpha_{13} = 0.5\,{\rm N/m}$, and $\alpha_{23} = 0.26\,{\rm N/m}$.[22,23] The lattice constants, mismatch strain, and elastic constants for GaAs, and $In_{0.3}Ga_{0.7}As$ are listed as follows:[24,25] for

*Supported by the National Basic Research Program of China, the National Natural Science Foundation of China under Grant No 51002052, the Key Project in Science and Technology of Guangdong Province under Grant No 2011A080801018, and the China Postdoctoral Science Foundation under Grant No 2013M531840.
**Corresponding author. Email: mssgzhang@scut.edu.cn; msgli@scut.edu.cn

GaAs, lattice constant $a = 5.6419$ Å, $c_{11} = 11.879 \times 10^{11}$ dyn/cm^2, $c_{12} = 5.376 \times 10^{11}$ dyn/cm^2, $c_{44} = 5.94 \times 10^{11}$ dyn/cm^2; for $In_{0.3}Ga_{0.7}As$, lattice constant $a = 5.76682$ Å, $c_{11} = 10.811 \times 10^{11}$ dyn/cm^2, $c_{12} = 5.121 \times 10^{11}$ dyn/cm^2, $c_{44} = 5.343 \times 10^{11}$ dyn/cm^2. In this work, 256×64 discrete grid points are employed with periodic boundary conditions applied along the x axis.

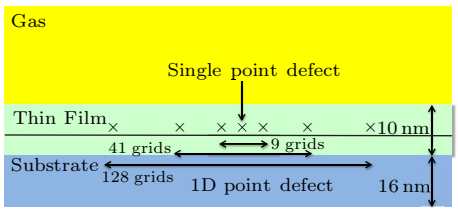

Fig. 1. Schematic illustration of a single point defect and a series of 1D point defects in plane located at the center of epitaxial thin film.

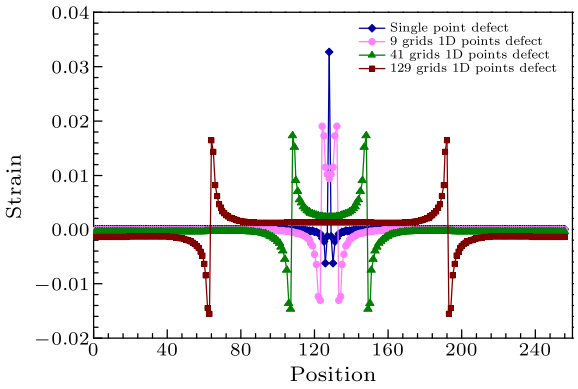

Fig. 2. The strain as a function of position along the solid line in Fig. 1. The circle, square, triangle, and cross symbol lines represents single defect, 1D defect of 9-grids, 41-grids, and 129 grids, respectively.

Figure 1 shows a schematic figure of point defects located in an epitaxial $In_{0.3}Ga_{0.7}As$ thin film. The thin film is assumed to be flat with an initial 10 nm thickness. A single point defect is placed at the center of the thin film. The value of the strain field along the solid line of Fig. 1 is plotted in Fig. 2. A sharp increase of the strain field is observed around the single point defect. We can also see significant oscillations around the point defect. To remove such oscillations in strain field, we propose to use a small one-dimensional (1D) point defect cluster for performing the strain field in a numerical simulation. Note that the 1D point defect cluster can also be considered as a dislocation loop in this 2D simulation. Three different defect cluster sizes of 9 nm, 41 nm and 129 nm are considered in the simulation. The calculated strain field of the defect clusters along the solid line, which is along the x-direction and is just one grid below the defect clusters, is also illustrated in Fig. 2. We can clearly see a decrease in the absolute value of the maximum local strain of point defect when the cluster size increases. When the defect cluster is in a large size of 129 nm, the local strain at the center of the defect cluster becomes zero, while a significant change of the strain field appears at the edge of the 1D defect cluster. These simulation results are in good agreement with the theoretical predictions and previous phase field simulations.

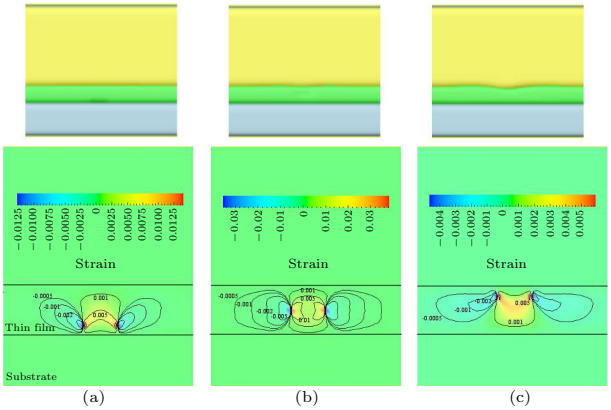

Fig. 3. The influence of the position of 1D point defects on the surface morphology. (a) The 1D point defects at the bottom of the thin film, (b) in the center of the thin film, (c) near the surface of the thin film. The first row shows the surface morphology, and the second row shows the strain distributions.

To explore the influence of the point defect on the surface morphology in $In_{0.3}Ga_{0.7}As$ thin film, we placed a 9 nm sized point defect at the bottom, center and the near-surface region of the thin film, respectively. The surface morphology and its corresponding strain field after 1000 steps evolution are shown in Figs. 3(a)–3(c). In the case of the defect at the bottom, it can be seen that there is a strong influence on the substrate/thin film interface, however, the defect cluster does not change the surface morphology. If this defect cluster is placed in the center of the thin film, a small oscillation can be seen on the surface morphology, as shown in Fig. 3(b). When this defect cluster is placed near the thin film surface, an undulation is clearly observed on the surface morphology. In the strain picture in Fig. 3, the strain contour plots show that the high strain field concentrates around the edge of the 1D defect clusters, with a compressive strain at the two sides of the cluster, and positive strain field is observed inside the 1D defect. As a static substrate is used in the simulation, we did not see any strain field in the substrate layer. It can be seen that a complete reflection symmetric strain field in the case of the defects in the center of the thin film. It should also be noted that in this case, the defect cluster generates a maximum strain field among the three cases. Even though the high strain field is introduced, its influence on the surface morphology is limited. Comparing Figs. 3(b) and 3(c), defects near the surface have a small strain field, while they result in a significant change of the thin film surface. This small strain field should be caused by the continuous interaction between the defects clusters and the surface morphology. According to the principle of minimum energy, the surface bending results in the increase of the interfacial energy, while avoid the high elastic energy introduced by the point defect clusters. Thus the total free energy decreases and the surface morphology changes.

Based on the simulation results, as can be seen, the point defects play critical roles in the surface kinetics of epitaxial growth. In particular, the point defects near the surface can lead to high roughness of the epitaxial thin film surface. In the following, the epitaxial thin film is initially set to have the amplitude of the sinusoidal surface profile

$$h(x) = h_0 + \beta \sin(kx + \phi), \tag{5}$$

where h_0 is the initial average thin film thickness; β is the amplitude, k is the wave numbers, and ϕ is the initial phase. In the following simulations, we chose $h_0 = 10\,\text{nm}$, $\beta = 5\,\text{nm}$, $k = 2\pi/32$ and $\phi = 0$.

The point defects are assumed to be randomly distributed in the thin film. The roughness of the thin film surface is then described by the rms roughness, which is defined as[26]

$$\text{rms} = \sqrt{\langle [h(x) - \bar{h}]^2 \rangle}, \tag{6}$$

where $\langle \cdots \rangle$ represents the average value of $[h(x) - \bar{h}]^2$, which is the mean height of the thin film surface. In the phase field model, we suggest the distance between the point where $\eta_1 = \eta_2 = 0.5$ and $\eta_2 = \eta_3 = 0.5$ as the height of the surface.

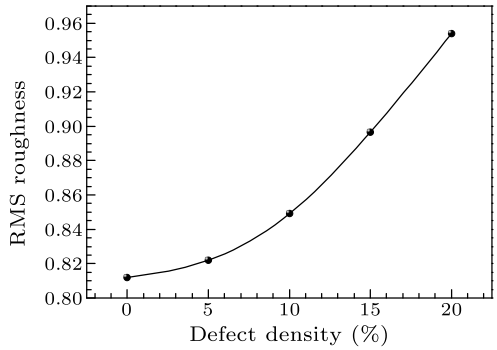

Fig. 4. Plot of the rms roughness as a function of the density of point defect with the defect magnitude fixed at 0.1. It is clearly demonstrated that the surface becomes rougher with the increase in the defect density.

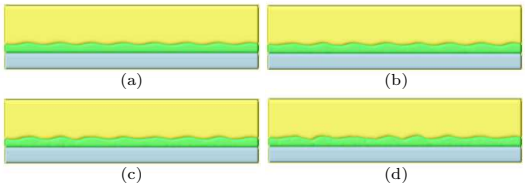

Fig. 5. (a)–(d) The surface morphology of $In_{0.3}Ga_{0.7}As$ thin film for 5%, 10%, 15%, and 20% defect density, respectively. The magnitude of the point defects is fixed at 0.1.

Firstly, let us study the influence of defect density on the surface morphology. Figure 4 shows the rms roughness versus point defect density at a fixed defect magnitude of 0.1. It is clearly demonstrated that the surface becomes rougher in the morphology profile with the increase of the defect density. The corresponding surface morphologies are present in Fig. 5. Compared to the defect-free surface profile (Fig. 5(a)), the surface morphology at a relatively small defect density 5% still shows a sinusoidal perturbation, and small changes are observed in the rms roughness (Fig. 5(b)). However, if the density of point defect increases to 20%, we note that the rms roughness increases very fast. In the surface morphology shown in Fig. 5(d), one can see the periodical sinusoidal perturbation disappears. This observation implies that the strain field driven by defect at a high density can disturb the surface diffusion process and increase the rms roughness.

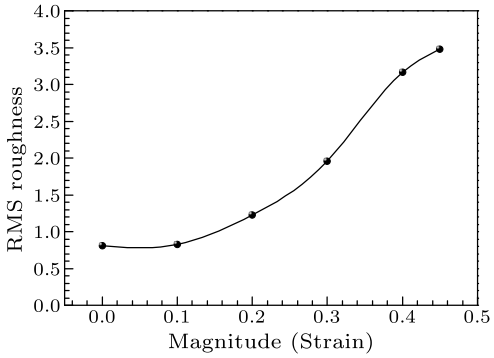

Fig. 6. Plot of the rms roughness as a function of the point defect magnitude, with the point defect density fixed at 5%. The rms roughness climbs quickly with the increase of defect magnitude.

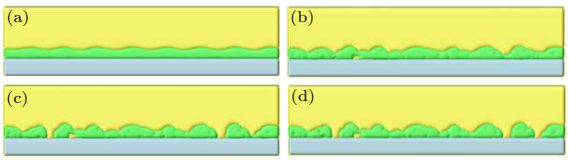

Fig. 7. (a)–(d) Simulated surface morphology for defect magnitude of 0.1, 0.2, 0.4, and 0.45, respectively. The point defect density is fixed at 5%. For a high defect magnitude, it is seen that the $In_{0.3}Ga_{0.7}As$ thin film surface is highly roughened with voids.

In the following studies, we investigate the effect of the magnitude of the point defects on the surface roughness. Hereby, the density of the point defect is maintained at 5%. By varying the magnitude of the defect from 0.1 to 0.45, the surface morphology dramatically changes. The rms roughness as the defect magnitude is shown in Fig. 6. For small disorder magnitudes (magnitude=0.1), the surface morphology is roughly similar to the defect-free surface with some small differences (Fig. 7(a)). As the magnitudes increase to 0.2, the thin film surface is roughened due to the preferential pinning on the defects. Interestingly, it should be noted that the gas phase (η_1) can be clearly seen in the thin film structure, as shown in Fig. 7(b). It is well known that introducing a new phase interface can increase the interfacial energy. However, the elastic energy induced by the point defect with large magnitude can dramatically decrease, and thus the total free energy will decrease and stay at a low level. The vacancy in the thin film avoids a strong elastic field induced by point defect while contributes to the surface roughness. Finally, for a very large disorder with the magnitude above 0.4, the fluctuations on the thin film surface exceed the thickness

of the thin film, resulting in a nanodot structure with a strong meandering, as seen in Fig. 7(c). It is therefore clear that the rms roughness reaches a very high value (∼3 nm) as a formation of nanodot structure. If the magnitude of the defect strain further increases, the rms roughness and the corresponding nanodot surfaces do not change significantly from the simulation results.

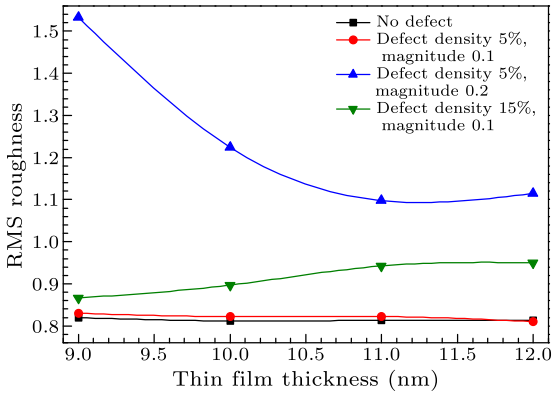

Fig. 8. Plot of rms roughness as a function of thin film thickness, with different defect densities and magnitudes. It is demonstrated that for point defects with high magnitude, thicker films can achieve high quality; in contrast, for point defects with high density, thinner films have a smooth surface.

Figure 8 illustrates how the thickness of the film affects the surface morphology for different defect distributions. The rms roughness increases slightly when a 5% density and 0.1 magnitude point defect is employed. However, if the magnitude of defects increases to 0.2, it can be seen that the surface roughness changes dramatically with the thin film thickness. These results indicate that thicker films can achieve high quality at a high level of point defect magnitude. In contrast, we perform simulations with high defect density (15%), it should be noted that the rms roughness increases with the increasing thickness of the thin film. This observation can be explained by the total number of defects. High defect density will introduce much more defects with the increase of thin film thickness, resulting in high rms roughness of the surface. This simulation shows that for point defects with high density, low thickness films have advantages on the surface quality due to the total number of defects associated with film thickness.

To examine the phase field simulation results, the surface morphology of $In_{0.3}Ga_{0.7}As$ thin films grown on GaAs substrates are demonstrated in our experiment. We consider two types of designed heterostructures. Type A: the $In_{0.3}Ga_{0.7}As$ epi-layers are grown on a GaAs substrate directly with the thickness of ∼20 nm under different growth conditions. Type B: the $In_{0.3}Ga_{0.7}As$ thin films are grown on GaAs substrates with four step-graded $In_xGa_{1-x}As$ buffer layers as reported in our previous work.[20] Details of the epitaxial growth process are presented in Ref. [20]. We now explore each of the two types for the surface morphology, which is characterized by scanning electron microscopy (SEM) and atomic force microscopy (AFM).

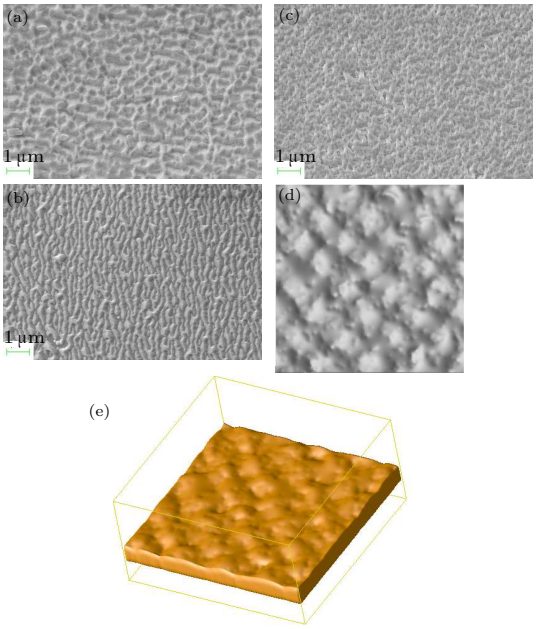

Fig. 9. SEM images of $In_{0.3}Ga_{0.7}As$ thin films grown at As_4 pressures of (a) 1.6×10^{-6} Torr, (b) 4.0×10^{-6} Torr, and (c) 1.5×10^{-5} Torr. It is seen that a high As_4 pressure can lead to a rough surface. The 3D phase field simulation results of surface morphology of $In_{0.3}Ga_{0.7}As$ thin film on GaAs substrate, with a defect density of 5% and magnitude of 0.2: (d) top view, in black/white, (e) 3D view. The simulated surface morphology is in exceptionally good agreement with the experimental results.

Type A: Figs. 9(a)–9(c) show the SEM images of the samples of type A with different As_4 pressures of 1.6×10^{-6}, 4.0×10^{-6} and 1.5×10^{-5} Torr, respectively. According to the works of Medel-Ruiz *et al.* and Yan *et al.*,[27,28] the growth of a strained material system generally undergoes a 2D→3D growth mode transition after only a few monolayers, and a plastic relaxation (dislocation or defect generation) occurs and leads to a degradation of optical/electronic properties. In our experimental works, for the sample grown at a low As_4 pressure of 1.6×10^{-6} Torr, the growth mode is 2D, and the sample has a low magnitude of defect. The surface of the $In_{0.3}Ga_{0.7}As$ thin film is only slightly roughened, as shown in Fig. 9(a). With the increase of the As_4 pressure, we observe a growth mode transition from a 2D layer to a 3D island growth, leading to an increase of the magnitude of point defect in the thin film. For a higher As_4 pressure of 4.0×10^{-6} Torr, the islands and pits are coalesced into fully formed ripple arrays (Fig. 9(b)), and for the highest As_4 pressure of 1.5×10^{-5} Torr, the $In_{0.3}Ga_{0.7}As$ thin film is highly roughened with trenches and voids, as shown in Fig. 9(c). The experimental results show that high As_4 pressure can lead to the increase of the magnitude of defect in the $In_{0.3}Ga_{0.7}As$ thin film, then the thin film growth mode undergoes a 2D→3D mode transition, and therefore, a rough surface is generated. These observations are consistent with our theory prediction, i.e., the magnitude of the defect can change the thin film surface morphology.

We also performed a 3D phase field simulation to

compare the simulation results to experimental observations. In this simulation, $128 \times 128 \times 64$ discrete grid points are employed. The defect density is fixed at 5% and a relatively high magnitude of 0.2 is used. As shown in Fig. 9(d), the surface morphology is in exceptionally good agreement with experimental results of Fig. 9(c), which proves that a higher magnitude of point defect strain field can lead to the increase in the surface roughness. A 3D view of the surface morphology is also illustrated in Fig. 9(e).

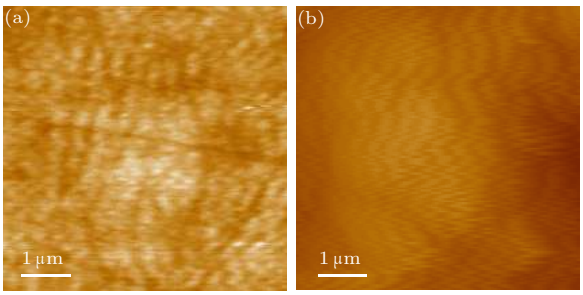

Fig. 10. AFM images of $In_{0.3}Ga_{0.7}As$ epi-layers with thickness of (a) 67 nm, (b) 133 nm. The view area is $5 \times 5\,\mu m$. The measured rms surface roughnesses are 1.2 and 0.62 nm, respectively. Higher thin film thickness can help to relax the in-plane stress and can lead to a low surface roughness.

Type B: to reduce the defect density in the $In_{0.3}Ga_{0.7}As$ thin film, a step graded $In_xGa_{1-x}As$ buffer layer is added between the $In_{0.3}Ga_{0.7}As$ thin films and the substrate. Three $In_{0.3}Ga_{0.7}As$ thin films of type B, at different thickness of 67, 100 and 133 nm, are grown on the GaAs substrate with buffer layers. Higher thin film thickness can help to relax the in-plane stress and can lead to a low-density defect for the thin film structure. Figures 10(a) and 10(b) show the surface AFM images ($5 \times 5\,\mu m$) of the $In_{0.3}Ga_{0.7}As$ layers with thicknesses of 67 and 133 nm, respectively. The measured rms surface roughnesses are 1.2 and 0.62 nm, respectively. Our previous experimental results[26] also demonstrated that a 100-nm-thick $In_{0.3}Ga_{0.7}As$ thin film with buffer layers has a small rms roughness of 0.56 nm. Obviously, the rms roughness decreases when a thick buffer layer is employed, which indicates that a low defect density can lead to smooth surfaces. Compared to the surface morphology with thin film thicknesses of 100 and 133 nm, we notice that with the further increase in thickness of buffer layer, there is a minor change in the rms surface roughness of the thin film due to the fact that the in-plane stress is fully relaxed on the top of the thin film. These experimental results also agree well with the phase field model. The $In_{0.3}Ga_{0.7}As$ thin films of higher thickness have low defect density and smooth surfaces.

In conclusion, the phase field model has been employed to predict and to study the surface morphology of InGaAs thin films in a point defect elastic system. Additional experimental works are performed to verify our phase-field simulation results. The surface morphology of 3D phase field simulation is in exceptionally good agreement with the experimentally achieved SEM images.

We thank Yang W J and Li J L for many helpful discussions.

References

[1] King R R, Law D C, Edmondson K M, Fetzer C M, Kinsey G S, Yoon H, Sherif R A and Karam N H 2007 *Appl. Phys. Lett.* **90** 183516
[2] Guter W, Schöne J, Philipps S P, Steiner M, Siefer G, Wekkeli A, Welser E, Oliva E, Bett A W and Dimroth F 2009 *Appl. Phys. Lett.* **94** 223504
[3] Wiemer M, Sabnis V and Yuen H 2011 *Proc. SPIE* **8108** 810804
[4] Luque A 2011 *J. Appl. Phys.* **110** 031301
[5] Kurtz S R, Myers D and Olson J M 1997 *IEEE The 26th Photovoltaic Specialists Conference* (Anaheim 29 September–03 October 1997) p 875
[6] Friedman D J, Geisz J F, Norman A G, Wanlass M W and Kurtz S R 2006 *The 4th World Conference on Photovoltaic Energy Conversion* (Hawaii 7–12 May 2006) p 598
[7] Geisz J F, Kurtz S R, Wanlass M W, Ward J S, Duda A, Friedman D J, Olson J M, McMahon W E, Moriarty T E, Kiehl J T, Romero M J, Norman A G and Jone K M 2008 *IEEE The 33rd Photovoltaic Specialists Conference* (San Diego 11–16 May 2008) p 1
[8] Sze S M 1981 *Physics of Semiconductor Devices* 2nd edn (New York: Wiley)
[9] Pillai M R, Kim S S, Ho S T and Barnett S A 2000 *J. Vac. Sci. Technol.* B **18** 1232
[10] Matthews J W and Blakeslee A E 1976 *J. Cryst. Growth* **32** 265
[11] Millunchick J M and Barnett S A 1994 *Appl. Phys. Lett.* **65** 1136
[12] Ashcroft N W and Mermin N D 1976 *Solid State Physics* (Orlando: Harcourt)
[13] Valtuena J F, Sacedon A, Alvarez A L, Izputa I, Calle F, Calleja E, MacPherson G, Goodhew P J, Pacheco F J, Garcia R and Molina S I 1997 *J. Cryst. Growth* **182** 281
[14] Haupt M, Kohler K, Ganser P, Emminger S, Muller S and Rothemund W 1996 *Appl. Phys. Lett.* **69** 412
[15] Ren Y Y, Xu B, Wang Z G, Liu M and Long S B 2007 *Chin. Phys. Lett.* **24** 2689
[16] Takano Y, Kobayashi K, Iwahori H, Kuroyanagi N, Kuwahara K, Fuke S and Shirakata S 2002 *Appl. Phys. Lett.* **80** 2054
[17] An Y P, Yang H, Mei T, Wang Y D, Teng J H and Xu C D 2010 *Chin. Phys. Lett.* **27** 017302
[18] Cahn J W and Hilliard J E 1958 *J. Chem. Phys.* **28** 258
[19] Khachaturyan A G 1983 *Theory of Structural Transformations in Solids* (New York: Wiley)
[20] Wu P P, Gao F L, Zhang K H L and Li G Q 2013 *RSC Adv.* **3** 3973
[21] Chen L Q and Shen J 1998 *Comput. Phys. Commun.* **108** 147
[22] Kurilo I V and Guba S K 2011 *Inorgan. Mater.* **47** 819
[23] Anan T, Nishi K and Sugou S 1992 *Appl. Phys. Lett.* **60** 3159
[24] Chuang S L 1995 *Physics of Optoelectronics Devices* (New York: Wiley)
[25] Mariager S O, Lauridsen S L, Dohn A, Bovet N, S ørensen C B, Schleputz C M, Willmott P R and Feidenhansl R 2009 *J. Appl. Crystallogr.* **42** 369
[26] Pelliccione M and Lu T M 2007 *Evolution of Thin Film Morphology Modeling and Simulations* (Berlin: Springer)
[27] Medel-Ruiz C I, Lastras-Martinez A and Balderas-Navarro R E 2003 *Phys. Status Solidi* C **0** 893
[28] Chokshi N, Bouville M and Millunchick J M 2002 *J. Cryst. Growth* **236** 563